


Please cite the Published Version

Khan, Junaid Ali, Khan, Muhammad Attique, Al-Khalidi, Mohammed , AlHammadi, Dina Abdulaziz, Alasiry, Areej, Marzougui, Mehrez, Zhang, Yudong and Khan, Faheem (2024) Design of Super Resolution and Fuzzy Deep Learning Architecture for the Classification of Land Cover and Landsliding using Aerial Remote Sensing Data. IEEE Journal of Selected Topics in Applied Earth Observations and Remote Sensing. pp. 1-17. ISSN 1939-1404

DOI: <https://doi.org/10.1109/jstars.2024.3490775>

Publisher: Institute of Electrical and Electronics Engineers (IEEE)

Version: Accepted Version

Downloaded from: <https://e-space.mmu.ac.uk/637066/>

Usage rights:  Creative Commons: Attribution-Noncommercial-No Derivative Works 4.0

Additional Information: This is an open access article published in IEEE Journal of Selected Topics in Applied Earth Observations and Remote Sensing.

Data Access Statement: Any kind of the data or code will be available on the specific request.

Enquiries:

If you have questions about this document, contact openresearch@mmu.ac.uk. Please include the URL of the record in e-space. If you believe that your, or a third party's rights have been compromised through this document please see our Take Down policy (available from <https://www.mmu.ac.uk/library/using-the-library/policies-and-guidelines>)

> REPLACE THIS LINE WITH YOUR MANUSCRIPT ID NUMBER (DOUBLE-CLICK HERE TO EDIT) <

Design of Super Resolution and Fuzzy Deep Learning Architecture for the Classification of Land Cover and Landsliding using Aerial Remote Sensing Data

Junaid Ali Khan, Muhammad Attique Khan (*Member, IEEE*), Mohammed Al-Khalidi (*Senior Member, IEEE*), Dina Abdulaziz AlHammadi, Areej Alasiry, Mehrez Marzougui, Yudong Zhang, (*Senior Member, IEEE*), Faheem Khan

Abstract— The diversity, noise, inter-image interference, image distortion and increase in the number of classes in aerial remotely sensed dataset cause exertion in the classification. The efficacy and stability of convolutional neural networks increase in image classification with the specified use of feature selection algorithm that causes remarkably improved decision making. To address the associated difficulties, a fuzzy deep learning architecture has been designed with a super resolution technique that consisting of 40 convolutional, four pooling, four inverted bottleneck blocks, and one fully connected layer. The fuzzy optimistic formula is implemented in 4 blocks as an activation function where information is fused from the previous layers and present block while the rest are using the ReLU transfer function to handle the issue of noise and inter-image interference. Feature selection is performed

based on the physics of chaotic particle swarm optimization hybrid with the active set algorithm. The accuracy of the proposed architecture is examined on three diverse datasets: Bije Earth Landslide/Non-Landslide, EuroSAT and NWPU-RESISC45, comprised of varying classes. The results are compared with state-of-the-art models like the hybrid version of VGGNet-16, Yolov4, ResNet-50, DenseNet-121 and other reported techniques. Moreover, the stability and computational complexity of the presented architecture are computed on 50 independent runs. It has been observed that the proposed architecture is stable, accurate, and viable and exploits a smaller number of learnable parameters than the models considered in comparison.

Funding: This work was supported through Princess Nourah bint Abdulrahman University Researchers Supporting Project number (PNURSP2024R508), Princess Nourah bint Abdulrahman University, Riyadh, Saudi Arabia. The authors extend their appreciation to the Deanship of Research and Graduate Studies at King Khalid University for funding this work through Large Research Project under grant number RGP2/283/45.

Corresponding: Mohammed Al-Khalidi (M.Al-Khalidi@mmu.ac.uk); Faheem Khan (faheem@gachon.ac.kr)

Junaid Ali Khan is with Department of Computer Science, HITEC University, Taxila, 47080 Pakistan (junaid.ali@hitecuni.edu.pk)

Muhammad Attique Khan is with Department of Artificial Intelligence, College of Computer Engineering and Science, Prince Mohammad Bin Fahd University, Saudi Arabia (attique.khan@ieee.org)

Mohammed Al-Khalidi is with Department of Computing and Mathematics, Manchester Metropolitan University, Manchester, UK (M.Al-Khalidi@mmu.ac.uk)

Areej Alasiry and Mehrez Marzougui are with College of Computer Science, King Khalid University, Abha 61413, Saudi Arabia (E: areej.alasiry@kku.edu.sa; mhrez@kku.edu.sa)

Dina Abdulaziz AlHammadi is with Department of Information Systems, College of Computer and Information Sciences, Princess Nourah bint Abdulrahman University, P.O.Box 84428, Riyadh 11671, Saudi Arabia (daalhammadi@pnu.edu.sa)

Yudong Zhang is with University of Leicester, Leicester, UK

Faheem Khan is with Department of Computer Engineering, Gachon University, Seongnam 13120, Republic of Korea (faheem@gachon.ac.kr)

Index Terms— Aerial Remote Sensing, Chaotic Particle Swarm Optimization, Fuzzy-CNN Deep Learning, Monte Carlo Simulations, Statistical Analysis and Model Stability.

I. INTRODUCTION

Aerial remote sensing (RS) plays a vital role in earth observation, getting images with high spatial resolution, monitoring geomorphological dynamics, disaster predictions and asset management [1]. The modern RS technologies involving multispectral imaging, light detection and ranging (LiDAR), aerial imagery, satellite imagery and unmanned aerial vehicles (UAV) etc [2] that's has applications in diverse fields like agriculture [3], biocybernetics [4] & biomedical engineering [5], climate monitoring [6], land use mapping and monitoring [7] but not limited. The quantitative facts and historical data leads towards the improved decision making at a reduced cost & error in prediction and analysis of earth observations and geographical worth [8]. In the early era of industry, the agents were manually inspected by an expert that have the chance of human error and it was unreal in terms of time, size of the problem, varieties of aerial views and number of classes in various datasets that gives birth to industrial revolution, utilization of computer vision approaches and intelligent decision support systems [9]. However, with the advent of

> REPLACE THIS LINE WITH YOUR MANUSCRIPT ID NUMBER (DOUBLE-CLICK HERE TO EDIT) <

computer vision frameworks industry 5.0 took birth and addresses the problem solving associated with various domain of engineering, science and technology like medical imaging, agriculture, gait analysis, image compression, segmentation, scene detection and many more [10].

The land use detection and classification have its own complexities and bottlenecks due to the complex background scene and interdependency of various scenes like farm & forest and river & sea side as shown in Figure 1.

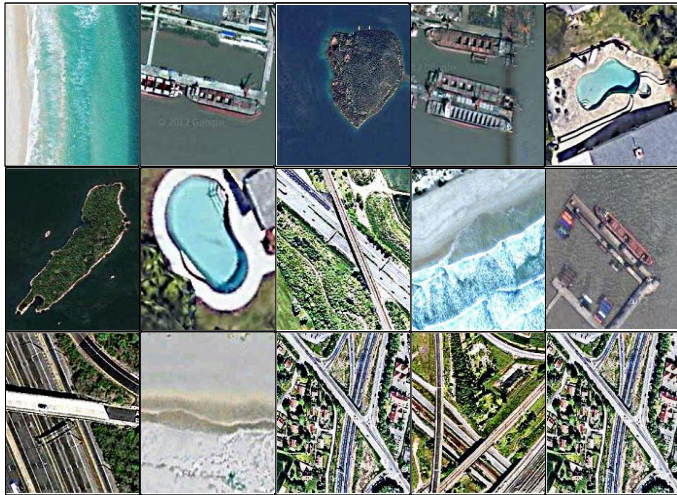


Figure 1: Samples high resolutions of the selected datasets

Moreover, the difficulties arise due to regions irregularity, high number of extracted features and multiple scene detection and classification [11]. The correctness of detected scene through a computer-based method involves, efficacy in preprocessing, outlying boundaries, effective feature extraction, dimensionality reduction and classification technique [12]. The applicability, effectiveness and stability of the machine learning (ML) technique depends upon the nature of dataset, problem complexity and distortion of the RS information [13]. In this regard, supervised learning is used for regression and classification problems that have labeled dataset while unsupervised learning is suitable for dimension reduction and clustering where the images have correlated attributes while reinforcement learning best suits the problems of control and classification [14]. Moreover, the development of sophisticated derivative free algorithm [15] addresses various non-linear, complex and tedious problems of agriculture, health care services, disaster management, industrial application and space technology. Deep learning is a subtype of machine learning and is introduced to handle high-dimensional problems such as imaging, videos, etc. Specially, convolutional neural networks (CNNs), have altered remote sensing by enabling automatic feature extraction from massive amounts of data, significantly improving tasks like land cover classification and object detection. While pre-trained models like VGG, ResNet, and EfficientNet have shown promise, they frequently fail in remote sensing applications because they are designed for general image datasets like ImageNet and do not account for remote sensing's unique challenges, such as scale

variation and spectral diversity. To tackle these challenges, we proposed a customized CNN based on four bottleneck and four inverted bottleneck blocks to reduce the computational complexity and preserve the critical information. The bottleneck block refines the feature and enhances the model's ability to process the complex remote sensing data. Keeping in view various difficulties associated with the data of earth observation and aerial scene classification, three datasets have been studied Bije earth landslide / non-landslide [16], NWPU-RESISC45 [10] and Eurostat [17], respectively. The main attributes including spatial resolution, number of images in each class, number of classes, and associated complications in these datasets are presented in Table 1 along with some of the sample images of each dataset.




The contributions of the presented work are as follows:

- A fuzzy optimistic formula base deep learning architecture is proposed that is consisting of 40 convolutional, 4 pooling, 4 inverted bottle neck blocks, 4 bottle neck blocks and one fully connected layer for land cover and land usage classification of RS data that ensures over fitting, provides reduced learnable parameters, lesser computational cost with higher level of accuracy.
- To address the complex and continuous nature of RS data, a fuzzy layer is included in the hidden layer of CNN for local and missing information extraction, curse of dimensionality and reduction of FNR. Moreover, the chaotic PSO is developed for optimized feature selection by introducing the chaos parameter γ in the velocity and position updating equations of the standard PSO algorithm.
- The results of the proposed architecture are compared with state of art models reported in the latest research provided in Table 2 by using various methods of ML and DL for different scene classification benchmark datasets on the performance indicator like accuracy, mean error, trainable parameters and computational complexity in term of time.
- The Monte Carlo simulations are performed based on sufficiently large number of independent runs to guarantee the applicability of the proposed scheme, reliability, convergence and computational complexity in term of time.

The rest of the article is outlined in such a way that detail of the dataset & its attributes, fuzzy based CNN framework, details of the performance indicator and chaotic PSO formulated for feature vector selection are presented in section III. The result and discussion along with the comparison with the state of art existed models are presented in section IV along with the parameter values and setting used in the simulations. In the last section the conclusions are drawn along with the directions of the future work.

> REPLACE THIS LINE WITH YOUR MANUSCRIPT ID NUMBER (DOUBLE-CLICK HERE TO EDIT) <

Table 1: Characteristics of various datasets and their samples

Disease Class	Characteristics	Few Samples
Bijie Earth Landslide/Non-Landslide [16]	The dataset is annotated with white for landslide and black for non-landslide with a resolution of 0.8m/pixel, it can be caused due to rock fall, debris flow and geologic material from a slopy surface. The initial sign of landslides involves ruptures of roads, heavy rainfall and displacement of trees that can be determined keeping in view the factors like elevation, curvature and sediment transport index [18].	
NWPU-RESISC45 [10]	It is scene classes dataset with reasonably large number of images having spatial resolution ranging from 20cm to more than 30m/pixel. The images have the difficulty of occlusion, illumination and class similarity [19]. The main classes are airfield, flyover, forest, river, farm, dense residential and some others that have inter scene interference and causes a difficulty for identification model to extract the features of the image to predict its class label.	
EuroSAT [17]	A benchmark dataset based on Sentinel-2 satellite images used to investigate the real strength of the deep learning architectures. The one of the difficulties is encapsulated in its 13 spectral bands having 27000 labeled and geo-referenced samples [20]. Keeping in view the high dimensionality of labeled classes, it is significant to use it after model training and then perform feature selection. The classes like annual crops, herbaceous vegetation and permanent crops causes interference and consequently difficulty in feature optimization.	

II. RELATED WORK AND STATE OF ART

Before the development of deep learning (DL), the ML techniques like support vector machine (SVM), AdaBoost, k-nearest neighbor (kNN), random forest and probabilistic neural networks (PNN) has gained much attention in the community of RS for the image classification, change detection and land cover estimation on a limited training samples with a compromised accuracy [21]. Some of the research employed machine learning, like Aziz et al. [22] suggested a machine framework for the classification of forest covering. The authors employed random forest, temporal stacked ANN layer using the Sentinel-2 dataset and they achieved 92.90% accuracy using random forest classifier and 97.75% accuracy using ANN algorithm. The limitation of this work was the high computation time for the training of the ANN algorithm using different configurations. However, with the advent of deep neural network (NN) architectures and DL the same problems have been addressed relatively with a greater level of accuracy, stability and lesser computational budget as it has larger potential of feature extraction and recognition by passing input data through several non-linearity functions in comparison with traditional shallow methods [23]. The deep feature extraction capability in the deep hidden layers of NN, compatibility of sophisticated optimization algorithms for feature optimization, pattern recovery and processing of unpredictable dataset make DL a powerful tool for RS data processing and useful decision making. The scientists have implied convolutional neural network (CNN) and its different versions like recursive CNN (R-CNN), faster

R-CNN, mask R-CNN assisted with an efficient global and or local optimizer as per problem nature to address RS image classification, land observation and land cover. Although lots of work has been exploited using DL, however, few of the related literature survey is presented to perform the gap analysis and establish the need for design of fuzzy based deep CNN Architecture hybrid with chaotic particle swarm optimization (C-PSO).

A constraint deep U-Net method [24] is presented by introducing auxiliary features of normalized difference vegetation index for mountain landslides dataset with varying window size and a precision of 88.87% has been obtained with a window size of 128×128. However, the precision is observed to be decreases with the decrease in size, eventually it is found to 71.94% for a window size of 64×64. In [25], COCO dataset of landslide / non-landslide has been taken with 160 images for training of both classes and 121 images for testing, moreover, the model is implemented by exploiting R-CNN capabilities incorporated with ResNet-50 and 101 as backbone models with 20 epochs and unitary batch size to get a recall of 0.93. The volume of dataset is observed to be small and some of the tarnished attributes like image background and distortion is not considered. A modified version of CNN called faster R-CNN [26] that uses skip connections to overcome the problem of gradient disappearance caused by excessive deep network has been implemented and compared with VGG16 and ResNet50 to get a precision of 69.59% that is better than that of VGG16 and ResNet50 on 120 epochs. RS multiple scene classification is a still challenging task due to complex composition of its images like palace and church

> REPLACE THIS LINE WITH YOUR MANUSCRIPT ID NUMBER (DOUBLE-CLICK HERE TO EDIT) <

that have similar global structure and special layout, in this regard various CNN models like VGGNet-16, DenseNet-161 and LDA based method has been exploited with batch size of 50, 15 and 15, respectively with varying weight density on NWPU-RESISC45 dataset [27]. Boreal landscape using Sentinel-2 dataset [28] has been exploited to classify the land cover and land use using various machine learning algorithms. Using the training testing ratio of 70:30 the results obtained by SVM, extreme gradient boosting, random forest and deep learning are (0.758 ± 0.017) , (0.751 ± 0.017) , (0.739 ± 0.018) and (0.733 ± 0.0023) , respectively. Shulong Jiang et. al [29] implied CNN as a feature extractor and XGBoost as classifier to get an accuracy of 95.5% and 83.35% for UC-Merced and NWPU-RESISC45 datasets, respectively. However, the results are obtained in a narrow domain by not considering the data from multi-sources and computational budget has not been presented. Similarly, the EuroSat data with 27000 labeled and geo-referenced images with 13 spectral bands that is comprised of ten classes is taken as a benchmark for deep CNN method to produce an overall classification accuracy of 98.57% [30], however the learnable parameters are quite high that leads towards the increased computational complexity. The wetland water areas classification is determined by Mehmet Akif Günen [17, 31] using ML based on SVM, linear discriminant analysis, K-nearest neighbor, AdaBoost and

canonical correlation forests techniques while DL is based on 1D CNN method while the results are compared with traditional performance measures. However, the performance of proposed CNN structure is not methodically considered. The state-of-the-art techniques presented by various researchers with which the results of the proposed architecture are compared are presented in Table 2 that describe the methodology used, level of accuracy achieved, dataset attributes and short coming or gap analysis. In this article fuzzy optimistic formula based deep layer is exploited in deep learning architecture whose features are optimized using C-PSO algorithm. The designed framework is applied on three different benchmark datasets having varying number of classes with multiple complex attributes. The results are compared on standard performance indicators with some of the existed pre-trained models as well as state of art techniques available in the literature in the latest half decade. The ablation study has been carried out keeping in view the variation in learning rate, mean square error study on various training to testing ratios, computational complexity in term of time and statistical evaluation based on 100 independent runs along with the comparison of the results with the pertained models as well as state of art techniques.

Table2: State of art work for comparison with the proposed architecture

Related work	Methodology	Accuracy (%)	Dataset Used
(Yang et al., 2024) [32]	Yolov4+SenseNet-121	93.46	Bijie Earth
(H Qin et al., 2024) [26]	Faster RCNN+ VGG-16	92.05	Landslide/Non-Landslide
(H Qin et al., 2024) [26]	Faster RCNN+ ResNet-50	93.80	[16]
(Cheng et al., 2017) [33]	VGGNet-16+ CNN Features	79.79±0.15%	NWPU-RESISC45 [10]
(Cheng et al., 2017) [34]	BoCF	84.32±0.17%	
(Cheng et al., 2018) [35]	D-CNN + VGGNet-16	91.89±0.22%	
(X Yang et al., 2020) [27]	VGGNet-16 + FPN	92.17±0.15%	
(Bhatt et al., 2024) [36]	Gaussian Naïve Bayes	60.21%	EuroSAT [17]
(Yamashkin et al., 2020) [37]	Geosystem Approach	91.52%	
(Eleni Kroupi et al., 2019) [38]	Deep CNN	86.00%	

III. MATERIAL AND METHODS

This section provides the details of the dataset used in the aerial scene study along with the proposed DL architecture that encapsulates the fuzzy based activation's function. Moreover, the mechanism adopted for the feature selection is also provided in the form of logical steps along with the performance metrics. The graphical workflow of the proposed methodology is presented in Fig. 2 which defines the complete procedure, transition layers, their skip connections, depth

connection, group convolution layer, additional layers, classification layer, fully connected layer, and the activation functions used at each level. The novel deep CNN is a network level fused model of customized CNN residual block architecture to explain the suggested framework for classification of Bijie Earth Landslide/Non-Landslide [16], NWPU-RESISC45 [10] and EuroSAT [17] datasets as illustrated in Fig. 2.

> REPLACE THIS LINE WITH YOUR MANUSCRIPT ID NUMBER (DOUBLE-CLICK HERE TO EDIT) <

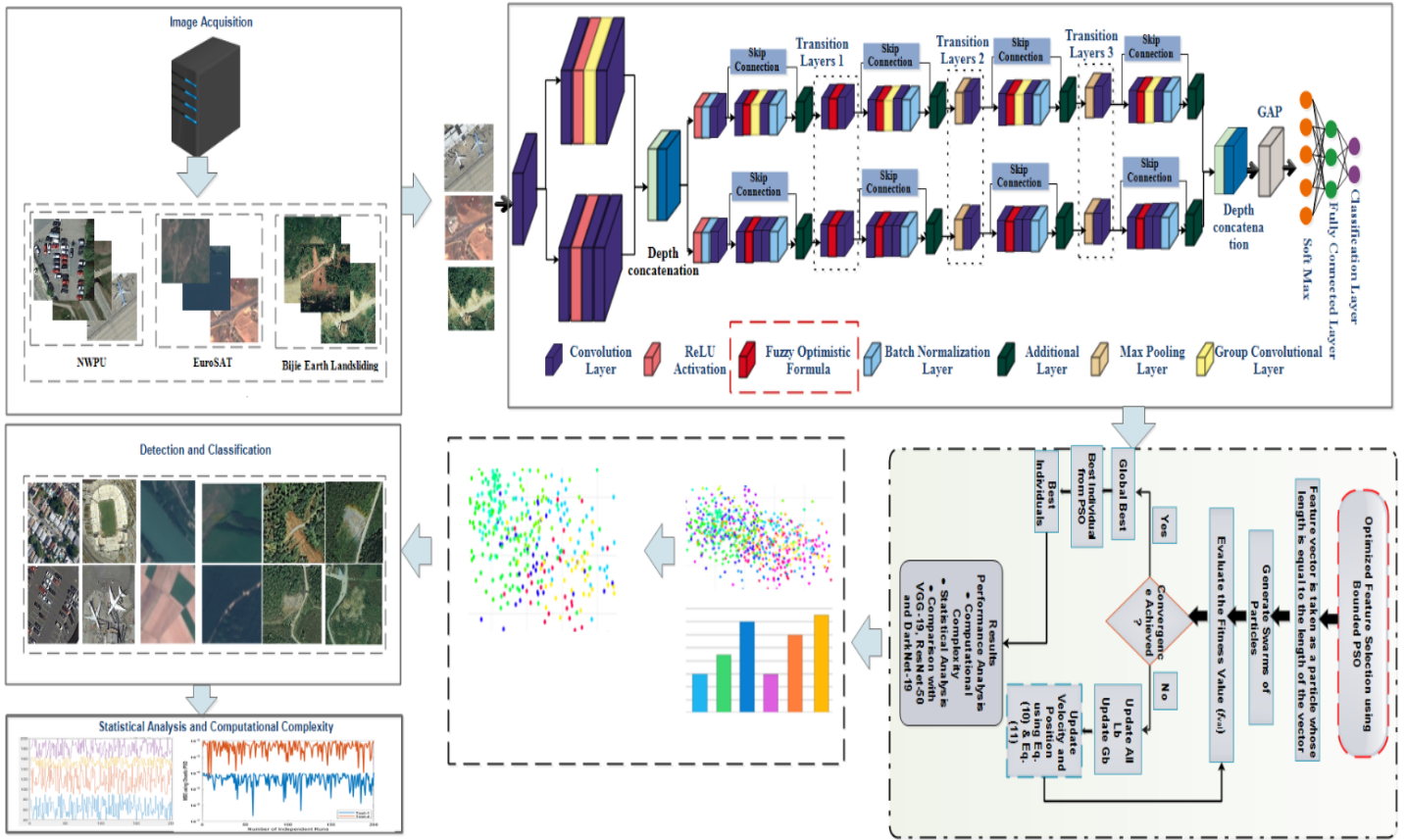


Fig.2. Graphical workflow of proposed methodology

A. Dataset Details

Three datasets have been used in the study in which the dataset of Bijie earth landsliding / non-landsliding have two classes with 770 landsliding and 2000 non-landsliding images. However, the dataset of NWPU-RESISC45 contains 12 classes and each class contains reasonable volume of the aerial images as provided in the Table 3. Moreover, the third dataset of EuroSAT have 10 classes of different land covers that contains the images as presented in Table 3. The nature of the dataset is complex and irregular that requires the applicability of deep learning, moreover keeping in view the noisy environment and background confusions fuzzy based activation has been exploited to overcome the drawbacks of the deep neural networks. Sufficient number of samples of each land use are taken so that the deep architecture model could learn and perform classification with a good prediction accuracy. The distribution of the inter image interference, damaged images, non-linear and outliers is uniform and well shuffled in the dataset. The other important characteristics like size of the dataset images and bit depth is also provided in the Table 1.

B. Proposed CNN Architecture

The suggested model was trained on training dataset using network level fusion is to improved and enhanced bounded, randomized C-PSO optimization for the optimal feature

selection. In the initial step image acquisition is performed on the selected datasets and then trained on the network level fusion of novel CNN based architectures of residual block. Furthermore, newly added depth-wise activation was used to retrieve the features from the trained model. To choose the optimal features, enhanced C-PSO optimization was also used. Neural network classifiers receive the refined features in order to perform the final classification. Statistical analysis and computational complexity are used in the last stage to assess how well the neural network classifier function, architecture, and chaotic PSO perform.

The aim behind selecting the bottleneck is to encapsulate the complex information while preventing overfitting and excessive model size. The inverted bottleneck allows the network to scale in terms of depth and accommodate different resource constraints. The detailed aspects of the designed DL model are that it is a novel network level fusion of modified CNN residual blocks-based architecture in which nine blocks make up the architecture that has one parallel block and eight series blocks, as shown in Figure 3. The input size of the suggested CNN is $224 \times 224 \times 3$. The first parallel block begins with the convolution layer and consists of three parallel convolution layers, batch normalization, and RELU activation, a Fuzzy layer with a kernel size of 3×3 and 8 depth sizes and 1×1 stride.

> REPLACE THIS LINE WITH YOUR MANUSCRIPT ID NUMBER (DOUBLE-CLICK HERE TO EDIT) <

Table 1: Description of selected remote sensing datasets

Dataset	Classes	Training Data (80%)	Test Data (20%)	Total Dataset	Size	Bit Depth
Bijie Earth Landslide/Non-Landslide	Landslide	616	154	770	256x256	4
	Non-Landslide	1600	400	2000		
NWPU-RESISC45	Airfield	1120	280	1400		
	Anchorage	560	140	700		
	Beach	560	140	700		
	Dense Residential	560	140	700		
	Farm	1120	280	1400		
	Flyover	560	140	700		
	Forest	560	140	700		
	Game Space	1120	280	1400		
	Parking Space	560	140	700		
	River	560	140	700		
	Sparse Residential	560	140	700		
	Storage Cisterns	560	140	700		
EuroSAT	Annual Crop	2400	600	3000		
	Forest	2400	600	3000		
	Herbaceous Vegetation	2400	600	3000		
	Highway	1600	400	2000		
	Industrial	2000	500	2500		
	Pasture	1600	400	2000		
	Permanent Crop	2000	500	2500		
	Residential	2400	600	3000		
	River	2000	500	2500		
Sea Lake	2400	600	3000			

Starting at max pool, the second series residual block is created. Convolution layers, RELU activation, and one batch normalization, Fuzzy layer with a depth size of 32 and a kernel size of 3×3 with a stride of 1 are connected to it. In the third inverted residual block which is start from max pool with two convolution layers,1 RELU activation and batch normalization, Fuzzy layer with a kernel size of 3×3 , depth size of 32 and 1×1 stride. The convolution layer, which is connected with three convolution layers and one RELU activation with one batch normalization, Fuzzy layer stride of one by one, kernel size of one by one, and depth size of thirty-six, sixty-four, ninety-six, is where the fourth series residual block begins. The fifth series inverted residual block starts from convolution layer which is further connected with two convolution layer and the remaining other layers of grouped convolution, RELU activation and batch normalization, Fuzzy layer with a stride of 1×1 , kernel size 1×1 and depth size is 32 and 96 respectively. The sixth series block starts with a convolution layer and is with further three convolution layers, 1 RELU activations, and one batch normalization layer, Fuzzy layer. The layers are coupled using a 64 and 96-depth size and a 1×1 kernel size with a stride of 1 and identical padding.

In the seventh inverted block comprises two convolution layers, one batch normalization layer, one RELU activation,1 grouped convolution, Fuzzy layer and one convolution layer at the beginning. Using a 1×1 kernel size with a stride of 1 and the same padding, the layers are connected using 96 and 256-depth sizes. Three convolution layers, one batch normalization layer, one RELU activation, one grouped convolution and one convolution layer at the beginning make up the 8th block. The layers are joined with 96,128 and 256-depth sizes using a 1×1 kernel size, a stride of 1, and the same padding. Furthermore, this architecture's last and final series inverted block begins with convolution layer and consists of two convolution layers, RELU activation, and a batch normalization layer, Fuzzy layer with a kernel size of 3×3 with a stride of 1 and minimum depth of 256. The two fusion-based networks that the depth concatenation is additionally attached to are fully connected, soft-max, and classification layer, respectively. The loss function of this model is categorical cross-entropy. The mathematical formula of loss function as $\varphi_{fL} = -\frac{1}{\delta_s} \sum_{k=1}^{\delta_s} \sum_{n=1}^L p_{kn} \text{Log}(T_{kn})$. Where δ_s is the number of samples, L is the number of classes, T_{kn} is denoted the predicted probability for class n , and p_{kn} denoted the actual labels such as 1 if true otherwise 0.

The suggested architecture contains 779.6K parameters, while the total comprises 101 layers, including 31 convolutional layers. Deep features were extracted from the depth

> REPLACE THIS LINE WITH YOUR MANUSCRIPT ID NUMBER (DOUBLE-CLICK HERE TO EDIT) <

concatenation layer after the proposed model had been trained on all three datasets. The proposed model's architecture layers are displayed in the Fig. 3 along with the layer structure and activation used.

S.No	Name	Activations	S.No	Name	Activations	S.No	Name	Activations
1	imageinput	227x227x3x1	36	batchnorm_5	57x57x32x1	68	conv_27	15x15x96x1
2	conv	114x114x8x1	37	addition_1_1	57x57x32x1	69	Fuzzy	15x15x96x1
3	conv_1	114x114x8x1	38	conv_14	29x29x64x1	70	relu_5_5	15x15x96x1
4	conv_2	114x114x8x1	39	Fuzzy	29x29x64x1	71	groupedconv_3	15x15x96x1
5	relu	114x114x8x1	40	relu_7	29x29x64x1	72	conv_28	15x15x128x1
6	relu_1	114x114x8x1	41	conv_15	29x29x64x1	73	batchnorm_9	15x15x128x1
7	conv_3	114x114x16x1	42	conv_16	29x29x32x1	74	addition_1_5	15x15x128x1
8	conv_4	114x114x8x1	43	Fuzzy	29x29x32x1	75	maxpool_2	8x8x128x1
9	groupedconv	114x114x8x1	44	relu_5_2	29x29x32x1	76	conv_29	8x8x128x1
10	batchnorm	114x114x16x1	45	conv_17	29x29x64x1	77	conv_30	8x8x96x1
11	batchnorm_1	114x114x16x1	46	conv_18	29x29x96x1	78	Fuzzy	8x8x96x1
12	batchnorm_2	114x114x16x1	47	batchnorm_6	29x29x96x1	79	relu_5_6	8x8x96x1
13	depthcat	114x114x32x1	48	addition_1_2	29x29x96x1	80	conv_31	8x8x128x1
14	maxpool	57x57x32x1	49	conv_19	29x29x96x1	81	conv_32	8x8x256x1
15	maxpool_1	57x57x32x1	50	conv_20	29x29x32x1	82	batchnorm_10	8x8x256x1
16	batchnorm_2	57x57x32x1	51	conv_21	29x29x32x1	83	addition_1_5	8x8x256x1
17	batchnorm_3	57x57x32x1	52	groupedconv	29x29x32x1	84	maxpool_2	4x4x256x1
18	conv_11	57x57x32x1	53	conv_22	15x15x128x1	85	conv_33	8x8x256x1
19	Fuzzy	57x57x32x1	54	conv_23	15x15x64x1	86	conv_34	8x8x96x1
20	relu_5_1	57x57x32x1	55	Fuzzy	15x15x64x1	87	relu_5_6	8x8x96x1
21	groupedconv	57x57x32x1	56	maxpool_2	15x15x96x1	88	Fuzzy	8x8x96x1
22	Fuzzy	57x57x32x1	57	maxpool_3	15x15x96x1	89	groupedconv_4	8x8x96x1
23	conv_12	57x57x32x1	58	conv_24	15x15x128x1	90	conv_35	8x8x256x1
24	batchnorm_3	57x57x32x1	59	conv_25	15x15x128x1	91	batchnorm_11	8x8x256x1
25	conv_6	57x57x32x1	60	Fuzzy	15x15x128x1	92	addition_1_5	8x8x256x1
26	conv_7	57x57x32x1	61	relu_5_1	15x15x128x1	93	maxpool_7	4x4x256x1
27	Fuzzy	57x57x32x1	62	conv_24	15x15x96x1	94	relu_5_6	4x4x256x1
28	relu_5	57x57x32x1	63	conv_25	15x15x128x1	95	relu_5_6	4x4x256x1
29	conv_9	57x57x64x1	64	conv_26	15x15x128x1	96	conv_36	4x4x512x1
30	conv_10	57x57x32x1	65	addition_1_4	15x15x128x1	97	conv_37	4x4x512x1
31	batchnorm_4	57x57x32x1	66	maxpool_2	8x8x128x1	98	depthcat_1	4x4x1024x1
32	addition_1	57x57x32x1	67	conv_25	15x15x128x1	99	depthcat_1	1x1x1024x1
33	conv_13	29x29x64x1				100	fc	10x1
34	Fuzzy	29x29x64x1				101	softmax	10x1
35	relu_6	29x29x64x1						

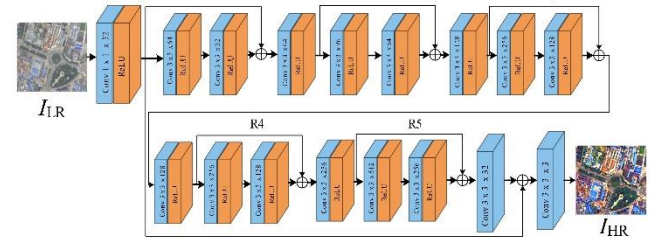
Fig.3. Layer structure and activations

B. Proposed 5 Block High Resolution Network (5B-DSR)

VSDR employs approaches like DCNNs to learn the mapping from sparse observations to high-resolution images. These models can discern intricate patterns and textures vital for efficient reconstruction. In this work, we proposed 5 residual-based CNNs to transform low-resolution images into high-resolution images. The network's input starts with a dimension of $224 \times 224 \times 3$ and has low resolution denoted with I_{LR} . After that, an initial convolutional layer is applied with 1×1 kernel size, 32 number of filters and 1×1 stride. After that, five residual blocks are attached. Every residual consist of two

convolutional and two ReLU activations. After each residual block, one convolutional layer is employed. Inside the residual blocks, the configuration of each convolutional is same such as 3×3 kernel size, 1×1 stride except the number of filters. The number of filters in the first residual block is 64 and 32, in second block 96 and 64, in third block is 128, and 96, in fourth and fifth block is 256,128, and 256,512 respectively. After that, post residual blocks convolutional is attached with configuration of 3×3 kernel size, 1×1 stride, and 32 number of filters. Furth more, the post residual convolutional is added with the initial convolutional layer to direct bypass the feature maps into the deep layer. In the last, another convolutional layer is added with 1×1 kernel size, 3 number of filters and 1×1 stride to refine the feature maps and output layer is regression layer with mean squared error loss function. The learnable parameters of the proposed 5C-DSR is 3.8 million with a total of 40 layers. The architecture of proposed 5C-DSR is presented in Figure 4.

Fig.4. architecture of the proposed 5C-DSR high resolution reconstruction network



Consider a training dataset $\{\varphi^i, \omega^i\}_{i=1}^S$, our aim to lean a M_{5DSR} model that predicts the value of $\hat{\vartheta} = M_{5DSR}(\varphi)$ where $\hat{\vartheta}$ the target value of I_{HR} . Using the training set, the loss mean square error $\frac{1}{2} \|\hat{\vartheta} - M_{5DSR}(\varphi)\|^2$ will be minimized. The resultant reconstructed high resolution samples are shown in Figure 5.

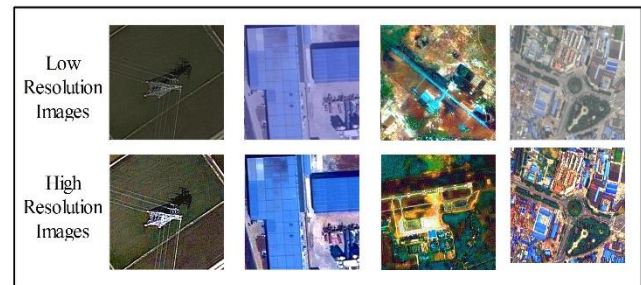


Fig. 5. Few samples of reconstruction of high resolution images using proposed 5C-DSR network

C. Proposed Fuzzy Deep Learning Architecture

The fuzzy optimistic formula [39] is introduced as an activation function in each transition layer as shown in Fig.1 to estimate the missing feature of the images accurately. The mathematical description along with optimistic formula is given below:

$$(Eq.1)$$

$$w \times \tau = \langle \mu_{w\tau}, v_{w\tau} \rangle =$$

> REPLACE THIS LINE WITH YOUR MANUSCRIPT ID NUMBER (DOUBLE-CLICK HERE TO EDIT) <

$\langle \max(\mu_w, \mu_\tau), \min(v_w, v_\tau) \rangle, \mu_\tau$ and $v_\tau \in [0,1]$
 $\langle I_1, I_2, \dots, I_m \rangle, \{ \langle \xi_1^i, \xi_2^i, \dots, \xi_m^i \rangle | 1 \leq i \leq \delta \},$
 $\{ \langle w_{j,1}^i, w_{j,2}^i, \dots, w_{j,m_i+1}^i \rangle | 1 \leq j \leq m_i \}, \{ \langle \beta_1^i, \beta_2^i, \dots, \beta_{m_i}^i \rangle \}$
 where δ is the number of layers of DNN; m_i is the number of neurons in the i^{th} layer; I_1, I_2, \dots, I_m is the input of the neuron; $\xi_1^i, \xi_2^i, \dots, \xi_m^i$ is the output of the neurons on the i^{th} layer, $w_{j,1}^i, w_{j,2}^i, \dots, w_{j,m_i+1}^i$ is the adaptive weigh coefficients mapping of j^{th} input to neurons in i^{th} layer; $\beta_1^i, \beta_2^i, \dots, \beta_{m_i}^i$ is the bias coefficients handling the noise in the i^{th} layer and $\psi_1^i, \psi_2^i, \dots, \psi_{m_i}^i$ is the fuzzy optimistic transfer function for the neurons in the i^{th} layer.

D. Feature Vector Selection using Chaotic PSO

The advantage of Chaotic PSO is that it introduces innovative, dynamic behavior in the search process. Incorporating chaotic sequences into PSO allows the algorithm to avoid being trapped in local optima, a common challenge in feature selection, especially within large and complex feature spaces. The optimal selection of the feature vector is performed by introducing the chaos parameter γ and chaos perturbation in standard PSO [40-42] velocity and positions updating equations given in Eq. (2) and Eq. (3), respectively.

$$v_i(n+1) = wv_i(n) + \gamma c1 \text{rand1}() \times (lb - X_i) \quad (\text{Eq.2})$$

$$+ \gamma c2 \text{rand2}() \times (gb - X_i)$$

Where w is the inertial factor and $c1$ & $c2$ are the balancing parameters for cognitive and social influences, $\text{rand1}()$ and $\text{rand2}()$ are coefficients generating the randomness in the search space.

$$X(n+1) = X(n) + \gamma v(n+1) \quad (\text{Eq.3})$$

While the chaos parameter corresponding to α_n is defined as:

$$\gamma: = \rho \alpha_n (1 - \alpha_n), \forall n = 0, 1, 2, \dots$$

where ρ is the controlling parameter that describe the chaotic dynamicity and trajectory of chaotic variable that is observed to be dense in the search space at $\rho = 4$. This chaos perturbation will sufficiently traverse the search space to introduce scatteredness in the feature selection and produces the optimal opportunity to get refine vector. The proposed optimization modification is presented in the form of logical steps:

Step 1: Initialization of the Particles

Create a primary swarm as a set of arbitrarily dispersed particles using constrained real values. The length of each particle is equivalent to the size of the selection feature vector and is considered as a candidate solution. The total number of iterations are 200.

Step 2: Formulation of Cost Function

The cost function formulated based on the performance indicator given in Eq. 2 and Eq. 3 and standard function available in literature for accuracy, F1-score and FNR. The fitness value is calculated for each unknown while the velocity and position of the unknown is updated by using the modified

standard equations of the PSO algorithm given in Eq. 2 and Eq. 3. The Fine-KNN is employed as a fitness function.

Step 3: Exit criteria

The execution of PSO has exit if any one of the following conditions fulfills

- Fitness value $\leq 10^{-10}$
- Pre-defined number of flights
- If the value of the global best does not change for 10 iterations
- Function tolerance = 10^{-12}

If termination criteria are met, then go to step 6 else continue.

Step 4: Ranking

Updated the global and local best particles of the swarm and ranked them according to the maximum fitness by performing the index sort.

Step 5: Renewal of particle by updating the velocity and position

Updated velocity and position of the particles by applying the chaos parameter γ and chaos perturbation on Eq. (2) and Eq. (3), respectively and repeat steps 2 to 5 until defined number of flights achieved.

Step 6: Data storage, analysis and Monte Carlo Simulations

- Store the weights of best particle as optimized features in a specific independent run.
- Store the best fitness values of the optimizer to see the effectiveness of chaotic PSO
- Store the execution time of the optimizer

For reliability, repeat steps 1 to 5 for a sufficiently large number of independent runs and perform the analysis.

Step 7: Refinement

The interior point algorithm is incorporated for speedy optimization by taking the best feature of chaotic PSO as a start point to the local search method. MATLAB built in environment is used for IPA as following procedure Updated velocity and position of the particles by applying the chaos parameter

E. Performance Indices of the Proposed Methodology

The standard performance indicators of dep learning have been used like accuracy, error, sensitivity, specificity, False Positive Rate, F1 Score [33]. The results of the proposed architecture and other state of art techniques are also computed using the same performance measure using the standard mathematical formulas given in the literature [34].

III. RESULTS AND DISCUSSION

The results of the proposed architecture are compared with pre-trained models as well as state of art techniques available in the literature as listed in Table 2 for different datasets. In this regard, the pretrained techniques that are compared with proposed framework are Alexnet, VGG19, ResNet50, Inception V3 and NasNet-large. However, the state of art techniques exploited for Bijie Earth Landslide/Non-Landslide dataset are Yolov4 hybrid

> REPLACE THIS LINE WITH YOUR MANUSCRIPT ID NUMBER (DOUBLE-CLICK HERE TO EDIT) <

with senseNet-121 [32], faster RCNN hybrid with VGG-16 & ResNet-50 [26], respectively. Moreover, the techniques like VGGNet-16 hybrid with CNN features [33], BoCF [34], D-CNN hybrid with VGGNet-16 [35] and VGGNet-16 hybrid with FPN [27] are compared with proposed scheme on NWPU-RESISC45 dataset and Gaussian Naïve Bayes [36], Geosystem approach [37] and deep CNN techniques [38] are applied on EuroSAT dataset, respectively.

The simulations are performed using MATLAB R2023b on the hardware with the specifications Intel (R) Core processor, 64 GB of RAM, 256 SSD with an integrated 1TB HDD, and an 8 GB NVIDIA RTX graphics card. The dataset is selected randomly 80% for training and 20% for testing by fixing a mini batch size of 16. The model has been trained for 100 epochs with a drop factor of 0.65 and a drop period of 6 parameters. The value of the learning is not fixed it has been varied from 10^{-04} to 10^{-02} in order to have adaptability during the training, moreover the other hyperparameters are presented in Table 4.

Table 4: Hyperparameter values and setting for simulations

Parameters	Value / Settings
Learning rate	$[10^{-4}$ to $10^{-2}]$
Optimizer	Chaotic PSO
Ratio of dataset	80(training): 20 (testing)
Drop period	6
Minimum batch size	64
Section depth	02
Objective value	0.156
L2 Regularization Factor	1.0×10^{-10}
No of Epochs	100
Option	Default

Moreover, the generic as well as specific parameter values and setting used for the optimization of feature selection is given in Table 5. In order to get a reasonable randomization and scatteredness in the search space a swarm of 200 particle is generated that has the length equal to the size of the feature vector of the images. The parameters of the local and global intelligence are defined as $C_1=2$ and $C_2=4$, respectively. The search space for the particle is bounded by taking the $V_{max}=0.4 \times \text{Bound}$ and controlling parameter for chaos as $\rho = 4$.

Table 5: Parameter values and setting for Chaotic PSO

Parameters	Value / Settings
Swarm Size	200
Particle length	As per size of the feature vector
Number of Flights	1500
C1	2
C2	4
Controlling Parameter	$\rho = 4$
Vmax	$0.4 \times \text{Bound}$
L2 Regularization Factor	1.0×10^{-10}
Options	Default

The parameter values given in Table 4 and Table 5 are used in the

entire simulations by considering all three datasets case wise.

A. Case I: Bijie Earth Landslide/Non-Landslide dataset

The deep features are extracted using the proposed architecture to perform an accurate classification for Bijie Earth Landslide/Non-Landslide dataset along with the basic feature parameters variation. The classification is performed using the different classifiers like N^3 , MN^2 , WN^2 , BN^2 and TN^2 respectively and the results are tabulated in Table 6 in terms of accuracy, recall, precision, F1 score, FNR, and computational complexity in terms of time. From the table, it is quite evident that the results of MN^2 is relatively better than that of other classifiers. Although the computational complexity in terms of time is 19.963 seconds which is higher than the other methods, however, the factor can be overhead keeping in view the reliability, accuracy, precision, and Recall.

Table 6: Classification results of proposed architecture on Bijie Earth Landslide/Non-Landslide dataset

Classifier	Accuracy	Recall	Precision	F1Score	Time (sec)
N^3	93.3	92	91.85	91.92	10.02
MN^2	93.5	91.8	92.5	92.14	19.96
WN^2	93.0	90.75	92.2	92.14	14.56
BN^2	92.9	90.9	91.75	91.32	10.05
TN^2	92.7	91.5	91.05	91.27	11.93

The confusion matrix for MN^2 classifier is given in the Fig. 6 that provide an accuracy of 96.00% for non-landslide and 87.6% for landslide images. The issue of the geological materials and resolution of 0.8m/pixel is classified with a reasonable accuracy and distinguishes the effects like rock fall, debris flow and slopy surfaces, respectively.

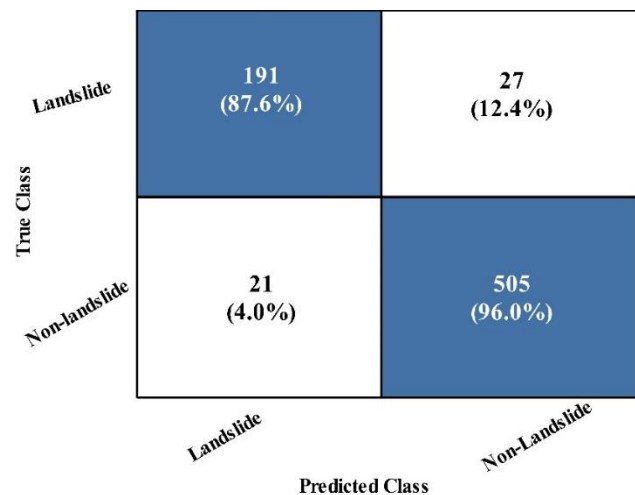


Fig. 6: Confusion matrix of MN^2 dataset for Bijie earth landslide / non-landslide dataset

B. Case II: EuroSat dataset

To see the reliability of the proposed architecture, the benchmark dataset of Sentinel-2 satellite images with fused spectral bands is trained using deep learning architecture. The classification results are presented in Table 7 using various

> REPLACE THIS LINE WITH YOUR MANUSCRIPT ID NUMBER (DOUBLE-CLICK HERE TO EDIT) <

standard classifiers and the highest accuracy of 93.3% is obtained using WN^2 technique. It is worth mentioning that the classes like annual crops, herbaceous vegetation, and permanent crops are distinctly separated and classified by the proposed scheme in 496.56 seconds which is significantly lesser than that of other classifiers reported in the table. Moreover, the lowest value of the accuracy is obtained using N^3 & BN^2 classifier which is still 89.6% which clearly explains the depth in the proposed fuzzy deep learning approach.

Table 7: Classification results of proposed architecture on EuroSat Dataset

Classifier	Accuracy	Recall	Precision	F1Score	Time (sec)
N^3	89.6	89.21	89.29	89.24	1565.1
MN^2	92.1	91.83	91.64	91.73	429.12
WN^2	93.3	93.06	93.07	93.06	496.56
BN^2	89.6	89.17	89.20	89.18	514.14
TN^2	89.7	88.93	88.86	88.89	694.61

The confusion matrix of EuroSat dataset is determined and presented in Fig. 7 in the form of true and predicted classes with an overall accuracy of 93.30%. From the figure, it is worth mentioning that even interdependent classes are also predicted correctly. However, the true prediction with highest individual accuracy is observed for the sea lake class due to its unique characteristics.

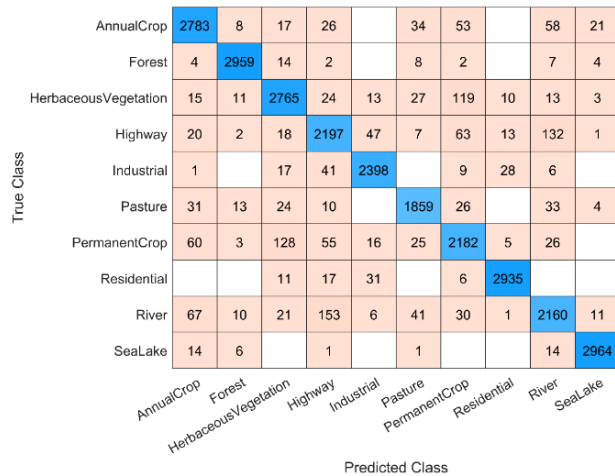


Fig 7: Confusion matrix of WN^2 classifier for EuroSat Dataset

C. Case III: NWPU-RESISC45 dataset

As a third case NWPU-RESISC45 dataset is trained on the same parameter values given in Table 5 and an accuracy of 90.5%, 92.8%, 93.3%, 90.8%, and 90.0% is obtained using the classifiers N^3 , MN^2 , WN^2 , BN^2 and TN^2 , respectively as tabulated in Table 8. The classification time of 100.22 seconds is observed for WN^2 classifier with an average accuracy of 93.40% which is quite comparable to that of the other presented techniques. A misclassification of 6.6% is obtained for WN^2 technique with a precision of 93.4%.

Table 8: Classification results of proposed architecture on NWPU-RESISC45 Dataset

Classifier	Accuracy	SEN	Precision	F1Score	Time (sec)
N^3	90.5	90.63	90.6	90.615	166.93
MN^2	92.8	92.89	92.98	92.935	70.904
WN^2	93.3	93.34	93.40	93.370	100.22
BN^2	90.8	90.82	90.95	90.887	324.91
TN^2	90.0	90.02	90.06	90.042	309.73

The depth of the fuzzy layer is examined by the confusion matrix as given in Fig.8 using WN^2 classifier for NWPU-RESISC45 dataset. From the matrix it is observed that the true prediction of the class game space is misled towards the dense and sparse residential class. Moreover, the true classes of the beach and anchorage is predicted correctly 692 and 696 images, respectively while few of the mislead classification is observed in these mentioned classes. Consequently, the scene classification with the difficulty of occlusion, illumination and image similarity with a spatial resolution from 20cm to 30m/pixel is performed with an accuracy of 90% to 93.3% that show supremacy of optimistic formula at the fuzzy layer to provide resistive effects against the noisy images.

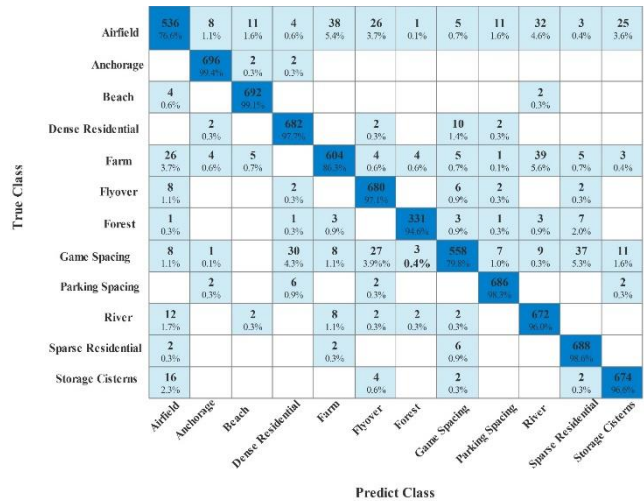


Fig 8: Confusion matrix of WN^2 classifier for NWPU-RESISC45 Dataset

D. Discussion

Ablation Study-1: The tradeoff between growth in the size of the deep structures, level of the accuracy, rate of convergence and computational budget required for deep learning model is pretentious by the learning rate. The effect on the accuracy and FNR is analyzed by varying the values of the learning rate from $[10^{-04}$ to $10^{-02}]$ on all three datasets trained and optimized by the proposed architecture. The results are tabulated in Table 9 by considering the values of the learning rate as 0.0013, 0.0135, 0.00013, and 0.00046, respectively. It is clear from the table that as the learning rate is decreasing the level of accuracy is increasing for all three datasets and the best level of accuracy is achieved at 0.00013. It is worth mentioning that the computational budget will increase but

> REPLACE THIS LINE WITH YOUR MANUSCRIPT ID NUMBER (DOUBLE-CLICK HERE TO EDIT) <

this effect can be mitigated while keeping in view the availability of sophisticated hardware.

Table 9: Analysis of proposed architecture results based on the change in learning rate

Learning Rate	Datasets			Performance Measure	
	Bijie Earth	EuroSAT	NWPU-RESISC45	Accuracy	FNR
0.00013	✓			93.50	6.5
		✓		93.30	6.7
			✓	93.34	6.66
0.0013	✓			91.56	8.44
		✓		90.48	9.52
0.00046	✓			89.23	10.77
		✓		88.50	11.5
			✓	87.09	12.91
0.0135	✓			84.52	15.48
		✓		87.20	12.8
			✓	84.29	15.71

Ablation Study-2: The reliability of feature optimization through C-PSO is analyzed based upon mean square error (MSE) of each independent run by considering different training to testing ratios for all three datasets. In this regard, sufficiently large number of independent runs are performed and the results are drawn in Fig. 9 on a semiology scale to see the effects of MSE in each run for all three datasets. Moreover, the results are also presented by taking training testing ratios of 80:20, 70:30, 60:40 and 50:50 as shown in Fig. 9 (a), Fig. 9 (b), Fig. 9 (c), and Fig. 9 (d), respectively. The stability in terms of MSE is observed once the vector selection is done by C-PSO hybrid with the proposed deep learning framework as presented in Fig. 6. It is quite evident from the figure that $MSE=10^{-1}$ to 10^{-07} is obtained for various training testing ratios of all three datasets, however the best value of the fitness is achieved in all four ratios for Beiji Earth dataset due to the nature and complexity in the images that that of NWPU-RESISC45 and EuroSAT datasets.

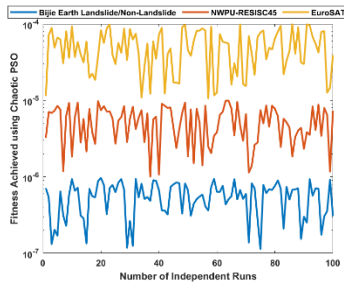


Fig. 9(a): Training: Testing =80:20

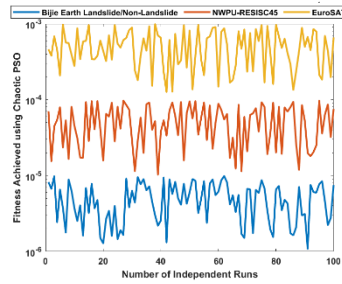


Fig. 9(b): Training: Testing =70:30

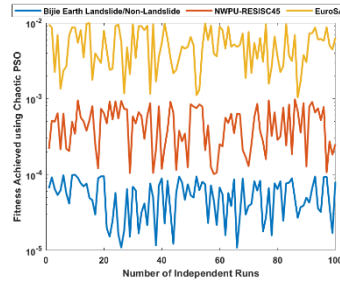


Fig. 9(c): Training: Testing =60:40

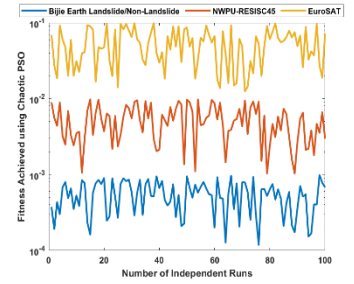


Fig. 9(d): Training: Testing =50:50

Fig.9 Behavior of MSE for various training and testing ratio using C-PSO for feature selection

Ablation Study-3: The overall precision, recall and F1-score is also calculated upto two decimal places for all three datasets and results are presented in Table. 10. The performance of the proposed model in term of accuracy and FNR are found to be in the range 93.34.91 % to 93.50% and 6.50% to 6.70%, respectively that is reasonably good keeping in view a complex classification problem of deep learning. The slight variation in the accuracy is due to variation of the number of classes in the dataset and their complexity level.

Table 10: Overall performance of the proposed model for Test-1and Test-2

Dataset	Performance Measures				
	Model		Overall		
	Accuracy %	FNR %	Precision	Recall	F1-Score
Bijie Earth	93.50	6.50	0.963	0.959	0.937
EuroSAT	93.30	6.70	0.949	0.938	0.942
NWPU-RESISC-45	93.34	6.66	0.942	0.921	0.939

Ablation Study-4: The computational complexity in term of time is calculated for various pre-trained models like Alexnet, VGG-19, ResNet-50, Inception V3, NasNet-large and compared with the proposed model for 100 independent runs. The results are presented in Fig. 10(a) for Beijiie Landslide / Non-Landslide dataset, Fig. 10(b) for EuroSAT, and Fig. 10(c) for the NPUW-RESISC45 dataset and compared with pre-d models. It is quite clear from the Fig. 10 that the computational budget in terms of time for the proposed model is quite comparable to that of the pre-trained reported models.

> REPLACE THIS LINE WITH YOUR MANUSCRIPT ID NUMBER (DOUBLE-CLICK HERE TO EDIT) <

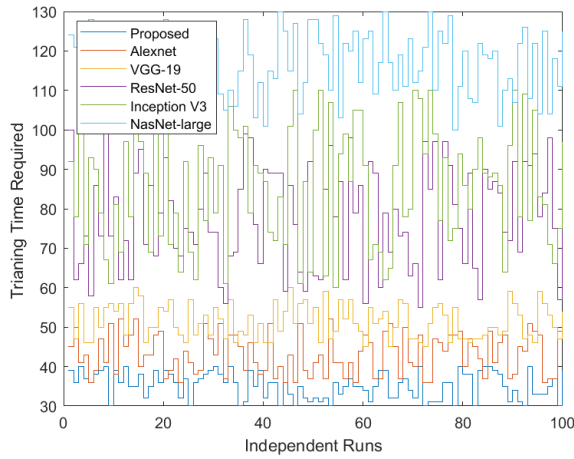


Fig.10 (a): Proposed model training time for Beijie Landslide / Non-Landslide dataset

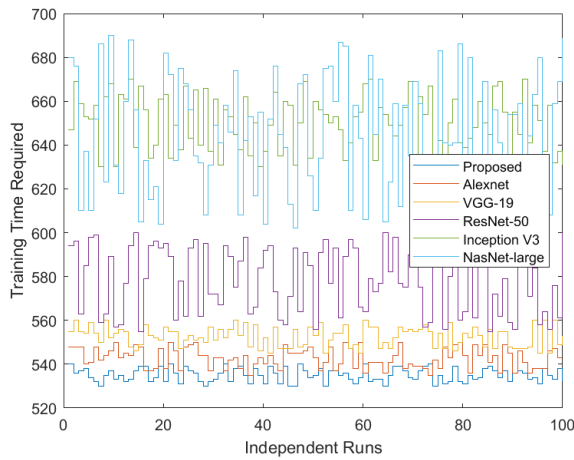


Fig.10 (b): Proposed model training time for EuroSAT dataset

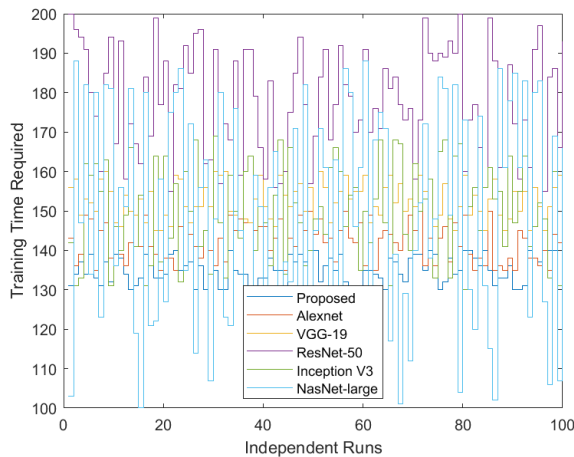


Fig.10 (c): Proposed model training time for NWPU-RESISC45 dataset

Fig.10 Comparison of computational complexity for proposed model and pre-trained models

The basic statistical indicators like minimum (Min), maximum (Max), mean (Mean), standard deviation (STD) and kurtosis is used to investigate the global values of the computational time in order to have the clear supremacy of the proposed approach. The results of the proposed as well as pre-trained models are

tabulated in Table 11 for all three datasets applied in the study.

Table 11: Proposed architecture statistical analysis for three datasets for 100 independent runs

Models	Statistical Performance Measure for 100 Independent Runs (seconds)				
	Beijie Landslide / Non-Landslide Dataset				
	Min	Max	Mean	STD	Kurtosis
Proposed	30.00	40.00	35.22	3.31	1.74
Alexnet	36.00	52.00	43.24	5.12	1.69
VGG-19	45.00	60.00	51.37	4.29	1.75
ResNet-50	55.00	100.0	78.08	12.76	1.84
Inception V3	60.00	110.0	85.80	14.89	1.87
NasNet-large	100.0	130.0	114.92	8.99	1.83
EuroSAT Dataset					
Proposed	530.0	540.0	534.91	3.03	1.91
Alexnet	535.0	550.0	542.26	4.98	1.53
VGG-19	545.0	560.0	552.48	4.37	1.81
ResNet-50	555.0	600.0	578.43	14.23	1.64
Inception V3	630.0	670.0	649.68	10.96	2.04
NasNet-large	600.0	690.0	650.42	25.83	2.07
NWPU-RESISC45 Dataset					
Proposed	130.0	140.0	135.12	3.34	1.71
Alexnet	135.0	150.0	141.80	4.72	1.78
VGG-19	145.0	160.0	152.57	4.62	1.79
ResNet-50	155.0	200.0	177.89	13.29	1.79
Inception V3	130.0	169.0	150.12	11.53	1.86
NasNet-large	100.0	189.0	145.29	25.36	1.83

Ablation Study-5: Fig.11 depicts the percent increase in the performance with the use of C-PSO optimized for various pre-trained models as well the proposed model for classification. One can observe that accuracy, precision, recall have increased and error has decreased. The negative sign (on right side of the graphs) in error values denotes that the error is reduced whereas, on left side positive values depict that accuracy, recall, specificity and precision have increased by using the C-PSO. The minimum increase in accuracy of 39% is exhibited by NasNet-large and maximum increase of 46.8% is shown by proposed model.

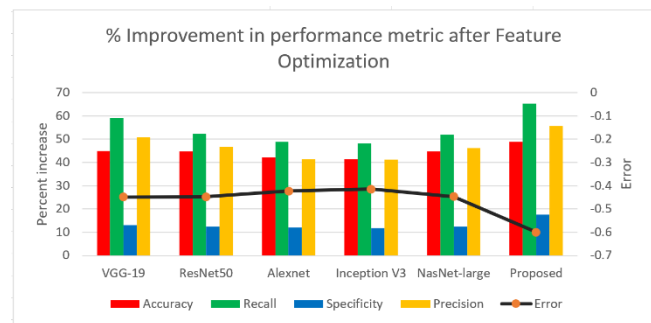


Fig.11 Illustration of percent increase and error decrease in classification by using C-PSO approach

Ablation Study-6:

> REPLACE THIS LINE WITH YOUR MANUSCRIPT ID NUMBER (DOUBLE-CLICK HERE TO EDIT) <

It is quite evident from Table 12 that the learnable parameters and size in megabytes for the proposed model are found to be reduced up to 6.3 million and 3.7 MB, respectively which is quite comparable to that of other models like VGG-19, ResNet-50, DarkNet-19, Inception-V3 as tabulated in the table.

Table 12: Comparison of learnable parameters of the proposed scheme and pre-trained models

Model	Depth	Size (MB)	Learnable Parameters (Millions)
Proposed	67	3.4	5.7
VGG-19	19	535	144
ResNet-50	50	96	25.6
DarkNet-19	19	78	20.8
Inception-V3	48	89	23.9

Comparison with State of Art and other Pre-Trained Models:

The performance measure in term of accuracy and FNR of the proposed architecture is compared with several pre-trained architectures & state of art reference techniques and the results are tabulated in Table 13. It is quite evident from the table that proposed architecture outperforms with an accuracy percentage of 93.5, 93.30, 93.34 and FNR percentage of 6.5, 6.7 and 6.66 for Beijie, EuroSAT and NWPU-RESISC45 datasets, respectively. The inclusion of fuzzy optimist formula offers subjective imaginations of the non-linear and missing detail of the images to get better decision accuracy and consequently the lesser FNR. Moreover, the accuracy and FNR of other pre-trained models and state of art reference results are also tabulated to establish a fair comparison. In Figure 12, lime technique is employed for the interpretation of proposed network.

Table 13: Comparison of the proposed architecture accuracy with several pre-trained and state of art models

Model	Datasets			Performance Measure	
	Beijie Eart h	EuroSA T	NWPU-RESISC45	Accurac y	FNR
Proposed Model	✓			93.50	6.5
		✓		93.30	6.7
			✓	93.34	6.66
Alexnet	✓			91.44	8.56
		✓		90.25	9.75
VGG19			✓	90.72	9.28
	✓			89.42	10.5
		✓		89.63	10.3
ResNet50			✓	90.51	9.49
	✓			88.53	11.4
		✓		89.11	10.8

			✓	89.04	10.9
InceptionV3	✓			90.62	9.38
		✓		89.84	10.1
			✓	90.14	9.86
NASNet-Large	✓			88.26	11.7
		✓		90.41	9.59
			✓	91.07	8.93
Yang et al [32]	✓			93.46	6.54
Bhatt et al [36]		✓		60.21	39.7
Cheng et al [33]			✓	79.79	20.2
H Qin et al [26]	✓			92.05	7.95
Yamashkin et al [37]		✓		91.52	8.48
Cheng et al [34]			✓	84.32	15.6
H Qin et al [26]	✓			93.80	6.2
Eleni et al [38]		✓		86.00	14.0
Cheng et al [35]			✓	91.89	8.11

IV. CONCLUSION

Based upon the comprehensive results supported with the graphs and tables followings conclusions are drawn:

- The proposed model produces lesser number of learnable parameters that are 5.7 million with a size of 3.4 MB and a depth of 67 which is quite lesser than that of other pre-trained models like VGG-19, ResNet-50, DarkNet-19 and Inception-V3 models.
- The minimum increase in accuracy of 39% is exhibited by NesNet-large and maximum increase of 46.8% is shown by proposed model when the feature vector is optimized with C-PSO algorithm. Moreover, it is worth mentioning that the accuracy, precision and recall have increased while the error has decreased by the inclusion of chaos parameter γ in standard PSO algorithm.
- An accuracy of 93.5%, 93.30%, 93.34% and FNR of 6.5%, 6.7% and 6.66% for Beijie, EuroSAT and NWPU-RESISC45 datasets, respectively are obtained from the proposed architecture which quite comparable with pre-trained models and state of art reported methods.
- The results obtained in the figures and tables by 100 independent runs deliver a guarantee about the applicability of the proposed model, reliability, convergence and computational complexity in term of time than that of sate of arts and pre-trained models, respectively.

The proposed work's limitation is that the hyperparameters for training are manually selected. In the future, we will employ a

> REPLACE THIS LINE WITH YOUR MANUSCRIPT ID NUMBER (DOUBLE-CLICK HERE TO EDIT) <

dynamical algorithm to select optimal hyperparameters and refine models that can reduce learnable parameters without compromising accuracy and computational budget.












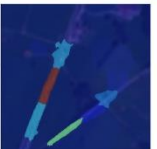
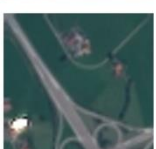










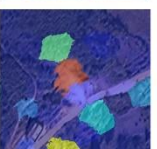
Proposed Network		
Input image	Predicted Image	Lime
NWPU-RESISC45 Dataset		
		
		
		
EuroStat Dataset		
		
		
		
Bijie Earth Landslide/Non-Landslide Dataset		
		
		

Fig.12 Performance of proposed network evaluating by employing Lime

ACKNOWLEDGMENT

This work was supported through Princess Nourah bint Abdulrahman University Researchers Supporting Project number (PNURSP2024R508), Princess Nourah bint Abdulrahman University, Riyadh, Saudi Arabia. The authors extend their appreciation to the Deanship of Research and Graduate Studies at King Khalid University for funding this work through Large Research Project under grant number RGP2/283/45.

Data Availability Statement: Any kind of the data or code will be available on the specific request.

REFERENCES

- [1] E. Alvarez-Vanhard, T. Corpetti, and T. Houet, "UAV & satellite synergies for optical remote sensing applications: A literature review," *Science of remote sensing*, vol. 3, p. 100019, 2021.
- [2] J. X. Yang, J. Zhou, J. Wang, H. Tian, and A. W. C. Liew, "LiDAR-Guided Cross-Attention Fusion for Hyperspectral Band Selection and Image Classification," *IEEE Transactions on Geoscience and Remote Sensing*, 2024.
- [3] I. M. Mehedi, M. S. Hanif, M. Bilal, M. T. Vellingiri, and T. Palaniswamy, "Remote Sensing and Decision Support System Applications in Precision Agriculture: Challenges and Possibilities," *IEEE Access*, 2024.
- [4] Y. Zhou, A. S. Mousavi, Y. R. Chalumuri, J. D. Parreira, M. Modak, J. A. Sanchez-Perez, *et al.*, "Inference-enabled tracking of acute mental stress via multi-modal wearable physiological sensing: A proof-of-concept study," *Biocybernetics and Biomedical Engineering*, vol. 44, pp. 771-781, 2024.
- [5] L. A. Ngiejungbwen, H. Hamdaoui, and M.-Y. Chen, "Polymer optical fiber and fiber Bragg grating sensors for biomedical engineering Applications: A comprehensive review," *Optics & Laser Technology*, vol. 170, p. 110187, 2024.
- [6] H. Han, Z. Liu, J. Li, and Z. Zeng, "Challenges in remote sensing based climate and crop monitoring: navigating the complexities using AI," *Journal of cloud computing*, vol. 13, p. 34, 2024.
- [7] B. Minasny, D. V. Adetsu, M. Aitkenhead, R. R. Artz, N. Baggaley, A. Barthelmes, *et al.*, "Mapping and monitoring peatland conditions from global to field scale," *Biogeochemistry*, vol. 167, pp. 383-425, 2024.
- [8] M. Heymann and A. Dahan Dalmedico, "Epistemology and politics in Earth system modeling: Historical perspectives," *Journal of Advances in Modeling Earth Systems*, vol. 11, pp. 1139-1152, 2019.
- [9] J. P. Shim, M. Warkentin, J. F. Courtney, D. J. Power, R. Sharda, and C. Carlsson, "Past, present, and future of decision support technology," *Decision support systems*, vol. 33, pp. 111-126, 2002.

> REPLACE THIS LINE WITH YOUR MANUSCRIPT ID NUMBER (DOUBLE-CLICK HERE TO EDIT) <

- [10] R. Fan, L. Wang, R. Feng, and Y. Zhu, "Attention based residual network for high-resolution remote sensing imagery scene classification," in *IGARSS 2019-2019 IEEE International Geoscience and Remote Sensing Symposium*, 2019, pp. 1346-1349.
- [11] T. Xu, Z. Guo, Y. Xia, V. G. Ferreira, S. Liu, K. Wang, *et al.*, "Evaluation of twelve evapotranspiration products from machine learning, remote sensing and land surface models over conterminous United States," *Journal of Hydrology*, vol. 578, p. 124105, 2019.
- [12] C. van Coller, "A Decision Support Tool for Implementing Machine Learning in SME Manufacturing Companies," Reutlingen University, Germany, 2024.
- [13] A. Albahri, Y. L. Khaleel, M. A. Habeeb, R. D. Ismael, Q. A. Hameed, M. Deveci, *et al.*, "A systematic review of trustworthy artificial intelligence applications in natural disasters," *Computers and Electrical Engineering*, vol. 118, p. 109409, 2024.
- [14] G. Obaido, I. D. Mienye, O. F. Egbelowo, I. D. Emmanuel, A. Ogunleye, B. Ogbuokiri, *et al.*, "Supervised machine learning in drug discovery and development: Algorithms, applications, challenges, and prospects," *Machine Learning with Applications*, vol. 17, p. 100576, 2024.
- [15] N. FUHS and T. Akiyama, "Evaluation of several schemes for classification of remotely sensed data," *Photogrammetric Engineering and Remote Sensing*, vol. 46, pp. 1547-1553, 1980.
- [16] S. Yang, Y. Wang, P. Wang, J. Mu, S. Jiao, X. Zhao, *et al.*, "Automatic identification of landslides based on deep learning," *Applied Sciences*, vol. 12, p. 8153, 2022.
- [17] M. A. Günen, "Performance comparison of deep learning and machine learning methods in determining wetland water areas using EuroSAT dataset," *Environmental Science and Pollution Research*, vol. 29, pp. 21092-21106, 2022.
- [18] W. G. Medwedeff, M. K. Clark, D. Zekkos, and A. J. West, "Characteristic landslide distributions: An investigation of landscape controls on landslide size," *Earth and Planetary Science Letters*, vol. 539, p. 116203, 2020.
- [19] S. Fang, K. Li, J. Shao, and Z. Li, "SNUNet-CD: A densely connected Siamese network for change detection of VHR images," *IEEE Geoscience and Remote Sensing Letters*, vol. 19, pp. 1-5, 2021.
- [20] K. Thiagarajan, M. Manapakkam Anandan, A. Stateczny, P. Bidare Divakarachari, and H. Kivudujogappa Lingappa, "Satellite image classification using a hierarchical ensemble learning and correlation coefficient-based gravitational search algorithm," *Remote Sensing*, vol. 13, p. 4351, 2021.
- [21] W. Han, X. Zhang, Y. Wang, L. Wang, X. Huang, J. Li, *et al.*, "A survey of machine learning and deep learning in remote sensing of geological environment: Challenges, advances, and opportunities," *ISPRS Journal of Photogrammetry and Remote Sensing*, vol. 202, pp. 87-113, 2023.
- [22] G. Aziz, N. Minallah, A. Saeed, J. Frnda, and W. Khan, "Remote sensing based forest cover classification using machine learning," *Scientific Reports*, vol. 14, p. 69, 2024.
- [23] L. Ma, Y. Liu, X. Zhang, Y. Ye, G. Yin, and B. A. Johnson, "Deep learning in remote sensing applications: A meta-analysis and review," *ISPRS journal of photogrammetry and remote sensing*, vol. 152, pp. 166-177, 2019.
- [24] G. Xu, Y. Wang, L. Wang, L. P. Soares, and C. H. Grohmann, "Feature-based constraint deep CNN method for mapping rainfall-induced landslides in remote regions with mountainous terrain: An application to Brazil," *IEEE Journal of Selected Topics in Applied Earth Observations and Remote Sensing*, vol. 15, pp. 2644-2659, 2022.
- [25] S. L. Ullo, A. Mohan, A. Sebastianelli, S. E. Ahamed, B. Kumar, R. Dwivedi, *et al.*, "A new mask R-CNN-based method for improved landslide detection," *IEEE Journal of Selected Topics in Applied Earth Observations and Remote Sensing*, vol. 14, pp. 3799-3810, 2021.
- [26] H. Qin, J. Wang, X. Mao, Z. a. Zhao, X. Gao, and W. Lu, "An improved faster R-CNN method for landslide detection in remote sensing images," *Journal of Geovisualization and Spatial Analysis*, vol. 8, p. 2, 2024.
- [27] X. Yang, W. Yan, W. Ni, X. Pu, H. Zhang, and M. Zhang, "Object-guided remote sensing image scene classification based on joint use of deep-learning classifier and detector," *IEEE Journal of Selected Topics in Applied Earth Observations and Remote Sensing*, vol. 13, pp. 2673-2684, 2020.
- [28] A. M. Abdi, "Land cover and land use classification performance of machine learning algorithms in a boreal landscape using Sentinel-2 data," *GIScience & Remote Sensing*, vol. 57, pp. 1-20, 2020.
- [29] S. Jiang, H. Zhao, W. Wu, and Q. Tan, "A novel framework for remote sensing image scene classification," *The International Archives of the Photogrammetry, Remote Sensing and Spatial Information Sciences*, vol. 42, pp. 657-663, 2018.
- [30] P. Helber, B. Bischke, A. Dengel, and D. Borth, "EuroSAT: A novel dataset and deep learning benchmark for land use and land cover classification," *IEEE Journal of Selected Topics in Applied Earth Observations and Remote Sensing*, vol. 12, pp. 2217-2226, 2019.
- [31] S. Ji, D. Yu, C. Shen, W. Li, and Q. Xu, "Landslide detection from an open satellite imagery and digital elevation model dataset using attention boosted convolutional neural networks," *Landslides*, vol. 17, pp. 1337-1352, 2020.
- [32] Y. Yang, Z. Miao, H. Zhang, B. Wang, and L. Wu, "Lightweight Attention-Guided YOLO With Level Set Layer for Landslide Detection From Optical Satellite Images," *IEEE Journal of Selected Topics in*

> REPLACE THIS LINE WITH YOUR MANUSCRIPT ID NUMBER (DOUBLE-CLICK HERE TO EDIT) <

- Applied Earth Observations and Remote Sensing*, 2024.
- [33] G. Cheng, J. Han, and X. Lu, "Remote sensing image scene classification: Benchmark and state of the art," *Proceedings of the IEEE*, vol. 105, pp. 1865-1883, 2017.
- [34] G. Cheng, Z. Li, X. Yao, L. Guo, and Z. Wei, "Remote sensing image scene classification using bag of convolutional features," *IEEE Geoscience and Remote Sensing Letters*, vol. 14, pp. 1735-1739, 2017.
- [35] G. Cheng, C. Yang, X. Yao, L. Guo, and J. Han, "When deep learning meets metric learning: Remote sensing image scene classification via learning discriminative CNNs," *IEEE transactions on geoscience and remote sensing*, vol. 56, pp. 2811-2821, 2018.
- [36] A. Bhatt and V. T. Bhatt, "Dcrff-Lhrf: an improvised methodology for efficient land-cover classification on eurosat dataset," *Multimedia Tools and Applications*, vol. 83, pp. 54001-54025, 2024.
- [37] S. A. Yamashkin, A. A. Yamashkin, V. V. Zanozin, M. M. Radovanovic, and A. N. Barmin, "Improving the efficiency of deep learning methods in remote sensing data analysis: geosystem approach," *IEEE Access*, vol. 8, pp. 179516-179529, 2020.
- [38] E. Kroupi, M. Kesa, V. D. Navarro-Sánchez, S. Saeed, C. Pelloquin, B. Alhaddad, *et al.*, "Deep convolutional neural networks for land-cover classification with Sentinel-2 images," *Journal of Applied Remote Sensing*, vol. 13, pp. 024525-024525, 2019.
- [39] V. Singh and S. P. Yadav, "Modeling and optimization of multi-objective programming problems in intuitionistic fuzzy environment: Optimistic, pessimistic and mixed approaches," *Expert Systems with Applications*, vol. 102, pp. 143-157, 2018.
- [40] J. A. Khan, M. A. Z. Raja, M. I. Syam, S. A. K. Tanoli, and S. E. Awan, "Design and application of nature inspired computing approach for nonlinear stiff oscillatory problems," *Neural Computing and Applications*, vol. 26, pp. 1763-1780, 2015.
- [41] I. Ahmed, A. R. Rao, A. Shah, E. Alamzeb, and J. A. Khan, "Performance of various metaheuristic techniques for economic dispatch problem with valve point loading effects and multiple fueling options," *Advances in Electrical Engineering*, vol. 2014, p. 765053, 2014.
- [42] M. M. Sabir and J. A. Khan, "Optimal design of PID controller for the speed control of DC motor by using metaheuristic techniques," *Advances in artificial neural systems*, vol. 2014, p. 126317, 2014.

Authors Bio

Junaid Ali Khan is currently a Professor/ Dean Faculty of Basic Sciences / Chairperson Computer Science Department, HITEC University Taxila. He completed his MS and PhD in Electronic

Engineering major in AI from Islamic International University, Pakistan in 2007 and 2011, respectively.

He has published 100+ research articles including few conferences and book chapters in renowned publishers like IEEE, Elsevier, SpringerLink, Hindawi and Willey. His area of interest is array signal processing, neural network modeling for non-linear systems, cognitive computation, complex hybrid optimization, Remote sensing image processing and medical imagery analysis. He is the reviewers of many journals such as Neurocomputing, Information Sciences, Soft computing, Information fusion, and Alexandria Engineering & many more

Muhammad Attique Khan: (Member IEEE) earned his Master's and Ph.D. degrees in Human Activity Recognition for Application of Video Surveillance and Skin Lesion Classification using Deep Learning from COMSATS University Islamabad, Pakistan in years 2018 and 2022, respectively. He is currently an Assistant Professor at Prince Mohammad Bin Fahd University. His primary research focus in recent years is medical imaging, COVID-19, MRI analysis, Video Surveillance, Human Gait Recognition, and Agriculture Plants using Deep Learning. He has above 280 publications that have more than 10,000+ citations and an impact factor of 850+ with h-index 61 and i-Index 165. He is reviewer of several reputed journals such as IEEE transaction on Industrial Informatics, IEEE transaction of Neural Networks, Pattern Recognition Letters, Multimedia Tools and Application, Computers and Electronics in Agriculture, IET Image Processing, Biomedical Signal processing Control, IET Computer Vision, Eurasipe Journal of Image and Video Processing, IEEE Access, MDPI Sensors, MDPI Electronics, MDPI Applied Sciences, MDPI Diagnostics, and MDPI Cancers.

Mohammed Al-Khalidi received the Ph.D. degree from the School of Computer Science and Electronic Engineering, University of Essex, Colchester, U.K., in 2018. He is a Senior Lecturer in Cyber Security and MSc Cyber Security Course Leader with the Department of Computing and Mathematics, Manchester Metropolitan University, Manchester, U.K. His past assignments include a Lecturer with the Department of Computer Science, Edge Hill University, and a Research Officer with the School of Computer Science and Electronic Engineering, University of Essex. Prior to that, he worked in industry as a Telecommunications Engineer at several leading mobile telecommunication companies in the Middle East & north Africa. He has more than ten years of industrial experience in mobile core network performance optimization. Dr. Al-Khalidi is a member of the British Computer Society.

Dina Abdulaziz AlHammadi received the Ph.D. degree from the University of Sheffield, Sheffield, U.K., in 2021. She is an Assistant Professor with the College of Computer and Information Sciences, Princess Nourah Bint Abdulrahman University, Riyadh, Saudi Arabia, specializing in artificial intelligence. Her research interests include AI, human computer interaction, personality recognition, and social AI. She is actively involved in mentoring students and collaborating with industry partners to bridge the gap between academia and practical applications of AI.

Areej Alasiry received the B.Sc. degree in information systems from King Khalid University, Abha, Saudi Arabia, and the M.Sc. degree (Hons.) in advanced information systems and the Ph.D. degree in computer science and information systems from Birkbeck College, University of London, U.K., in 2010 and 2015, respectively. She is currently an Assistant Professor at the College of Computer Science, King Khalid University. She also holds the position of the College Vice Dean for Graduate Studies and Scientific Research. Her main research interests include machine learning and data science.

> REPLACE THIS LINE WITH YOUR MANUSCRIPT ID NUMBER (DOUBLE-CLICK HERE TO EDIT) <

Mehrez Marzougui was born in Kasserine, Tunisia, in 1972. He received the B.Sc. degree from the University of Tunis, Tunisia, in 1996, and the M.Sc. and Ph.D. degrees from the University of Monastir, Monastir, Tunisia, in 1998 and 2005, respectively, all in electronics. From 2001 to 2005, he was a Research Assistant with Electronics and Micro-Electronics Laboratory. From 2006 to 2012, he was an Assistant Professor with Electronics Department, University of Monastir. Since 2013, he has been an Assistant Professor with Engineering Department, College of Computer Science, King Khalid University, Abha, Saudi Arabia. He is the author of more than 30 articles. His research interests include hardware/software cosimulation, image processing, and multiprocessor systems on chips.

Yudong Zhang received the Ph.D. degree from Southeast University, China, in 2010. He held a postdoctoral position, from 2010 to 2012, and was a Research Scientist, from 2012 to 2013, with the Research Foundation in Mental Hygiene, Columbia University, USA. From 2013 to 2017, he served as a Professor with Nanjing Normal University, where he was the Director and the Founder of the Advanced Medical Image Processing Group, NJNU. Since 2017, he has been a Professor (permanent) with the Department of Informatics, University of Leicester, U.K. His research interests include deep learning in communication and signal processing, and medical image processing.

Faheem Khan received the bachelor's degree from the University of Peshawar, Pakistan, in 2009, and the Ph.D. degree in computer science from the University of Malakand, Pakistan, in 2017. He is currently an Assistant Professor with Gachon University, South Korea. He is the author/coauthor of more than 30 publications in technical journals and conferences. His research interests include computer networking, information technology, sensor networks, wireless networks, mobile ad-hoc networks, the IoT, AI, and social networks.